Journal of Physics: Conference Series

PAPER • **OPEN ACCESS**

Structure and magnetic properties of $LiNi_{1-x}Co_xPO_4$ magnetoelectrics with x = (0, 0.1, and 0.2)

To cite this article: M A Semkin *et al* 2019 *J. Phys.: Conf. Ser.* **1389** 012050

View the article online for updates and enhancements.

IOP ebooks™

Bringing together innovative digital publishing with leading authors from the global scientific community.

Start exploring the collection–download the first chapter of every title for free.

This content was downloaded from IP address 212.193.78.232 on 06/10/2020 at 05:46

Structure and magnetic properties of $LiNi_{1-x}Co_xPO_4$ magnetoelectrics with x = (0, 0.1, and 0.2)

M A Semkin[1,2,*], N V Urusova[1,3], S Lee[4], M O Kalinkin[3], D K Kuznetsov[1], N A Kulesh[1], D S Neznakhin[1], D G Kellerman[1,3] and A N Pirogov[1,2]

[1]Institute of Natural Sciences and Mathematics of the Ural Federal University, 620002 Ekaterinburg, Russia
[2]M.N. Mikheev Institute of Metal Physics of Ural Division of RAS, 620108 Ekaterinburg, Russia
[3]Institute of Solid State Chemistry of the Ural Branch of the RAS, 620990 Ekaterinburg, Russia
[4]Korea Atomic Energy Research Institute, 305353 Daejeon, Republic of Korea

[*]E-mail: m.a.semkin@urfu.ru

Abstract. We present the magnetic properties of $LiNi_{1-x}Co_xPO_4$ magnetoelectrics, with x = (0–0.2), and their analysis of concentration dependences. Samples have been synthesized by a glycerol-nitrate method. To refine crystal structure X-ray diffraction measurements were carried out. Magnetic measurements were performed at the external magnetic field of 500 Oe over the temperature range (2–300) K. The neutron powder diffraction patterns of $LiNi_{0.9}Co_{0.1}PO_4$ were recorded over temperature interval from 4.4 K up to 25 K. The partial doping in the $LiNi_{1-x}Co_xPO_4$ magnetoelectrics the Ni ions for Co ions leads to a narrowing of the temperature interval where the incommensurate phase is established.

1. Introduction

Investigations of multiferroics those simultaneously exhibit multiple ferroic order parameters [1] actively have been performed in the past decade. Magnetoelectrics (ME) are the materials, where such coexisting order parameters couple ferroelectricity with magnetization under external magnetic field. They have also experienced a revival of interest due to the scientific challenges to unravel the coupling mechanism [2], as well as for their potential applications [3]. In $LiMPO_4$ (*M* = Ni, Co, Fe, Mn) the ME effect appear in their low-temperature antiferromagnetic (AFM) phases [4] with high liner magnetoelectric effect $\alpha \leq 2.0$ pS/m [5]. To explain the magnetoelectric effect in these materials, a model of spin-orbit interaction [4] or a model based on the Dzyaloshinsky-Moriya interaction [4] are usually used. The last causes a deviation of magnetic moments from the easy magnetization axis.

Except $LiNiPO_4$, in other $LiMPO_4$ there is a spontaneous transition from a commensurate (C) AFM phase to a paramagnetic state. The polarization arises at the temperature that is equal to the Néel point (T_N) [6]. This fact indicates a strong interaction between magnetic and ferroelectric degrees of freedom. In $LiNiPO_4$ a polarization exists only in the temperature interval, where the C magnetic phase takes place [7]. Further heating of the sample induces magnetic phase transition to an incommensurate (IC) structure at $T_{C\text{-}IC}$ = 20.8 K and then to the paramagnetic state at T_N = 21.8 K [8, 9]. The C AFM structure of the orthophosphates $LiMPO_4$ is described by the propagation vector $\boldsymbol{k_C} = 0$. For example, in the case of the commensurate structure of $LiNiPO_4$ magnetic moments of Ni

Content from this work may be used under the terms of the Creative Commons Attribution 3.0 licence. Any further distribution of this work must maintain attribution to the author(s) and the title of the work, journal citation and DOI.
Published under licence by IOP Publishing Ltd

ions, located at positions (0.25+*x*, 0.25, –*z*) and (0.25–*x*, –0.25, 0.5–*z*), are oriented along the *c*-axis and antiparallel to each other as well as to the moments at sites (–0.25–*x*, –0.25, *z*), and (–0.25+*x*, –0.25, 0.5+*z*); where $x = 0.026$, $z = 0.018$ [4].

The C structures of other orthophosphates differ from this structure for mutual orientations of moments or their directions relatively the crystallography axes. For instance, the spins are oriented along the *a*-axis in $LiMnPO_4$, and along the *b*-axis in $LiCoPO_4$ [10, 11]. The IC antiferromagnetic structure of $LiNiPO_4$ is described by propagation vector $\boldsymbol{k_{IC}} = 2\pi/b(0, 1\pm\tau, 0)$ with $\tau = (0.070–0.120)$ reciprocal lattice units (r.l.u.) [4]. A magnetic moment of the Ni ion has the *z* component alone. So, the IC structure can be represented as a transfer spin wave, moved along the *b*-axis.

Therefore, the aim of this work is a study of the structure and magnetic properties of $LiNi_{1-x}Co_xPO_4$ magnetoelectrics with x = (0, 0.1, and 0.2).

2. Experimental details

The $LiNi_{1-x}Co_xPO_4$ magnetoelectrics have been synthesized by a glycerol-nitrate method. The main advantage of this method is that the amount of gases emitted during the reactions leads to the dispersion of the product, which can lead to particles from 10 nm up to 10 μm in size.

X-ray diffraction (XRD) measurements were carried out at room temperature using Shumadzu diffractometer (X-ray source Cu K_α, $\lambda = 1.5418$ Å) at the Institute of Solid State Chemistry. Structural parameters were refined by Rietveld method using Fullprof program [12].

Morphology of the prepared powder samples was identified by scanning electron microscopy (SEM) AURIGA CrossBeam. The chemical composition ($Ni_{1-x}Co_x$) was measured using a full reflection Nanohunter X-ray fluorescence spectrometer in the Ural Federal University.

Magnetic measurements were performed with Magnetic Property Measurement System (MPMS XL-7) over the temperature range (2–300) K, under the applied magnetic field of 500 Oe, in the zero field cold (ZFC) mode. The (2–25) K and (25–300) K intervals were investigated with the step 0.02 K and 1 K, respectively.

The neutron powder diffraction (NPD) patterns at low temperatures were recorded with the HRPD diffractometer at the HANARO reactor in the Korea Atomic Energy Research Institute. The wavelength of the incident beam was $\lambda = 1.835$ Å.

3. Results

Figure 1 shows the XRD-patterns for $LiNi_{1-x}Co_xPO_4$ with x = (0, 0.1, and 0.2). All the observed reflections correspond to the *Pnma* space group. The lattice constants, ion coordinates, occupation coefficients and other structure parameters have been refined. As example, the lattice constants and agreement factors are presented in Table 1, the global agreement factors are less 3.2 %. The unit cell size increases with rising cobalt concentration in $LiNi_{1-x}Co_xPO_4$.

Table 1. A simple table. Unit cell parameters of crystal structure of the $LiNi_{1-x}Co_xPO_4$. R_f and χ^2 are Bragg and global agreement factors.

Parameter	x = 0	x = 0.1	x = 0.2
a (Å)	10.0335(6)	10.0513(6)	10.0697(6)
b (Å)	5.8581(3)	5.8646(3)	5.8722(4)
c (Å)	4.6785(3)	4.6811(3)	4.6839(3)
V (Å^3)	274.99(3)	275.94(3)	276.97(3)
R_f (%)	3.0	2.5	2.8
χ^2 (%)	3.2	2.7	3.1

The X-ray fluorescence analysis was performed to confirm of the chemical composition ($Ni_{1-x}Co_x$). Figure 2 shows the normalized X-ray fluorescence spectra on the Ni K_α intensity for $LiNi_{1-x}Co_xPO_4$ with x = (0, 0.1, and 0.2). Refined values of the cobalt content in the samples do not exceed 1 % in compare with nominal concentration.

Figure 3 displays the SEM-images of the $LiNi_{1-x}Co_xPO_4$ with x = (0–0.2). The image shows that $LiNi_{0.8}Co_{0.2}PO_4$ contains homogeneous particles with average sizes from 0.5 μm up to 50 μm. Similar SEM-images have been recorded for other samples.

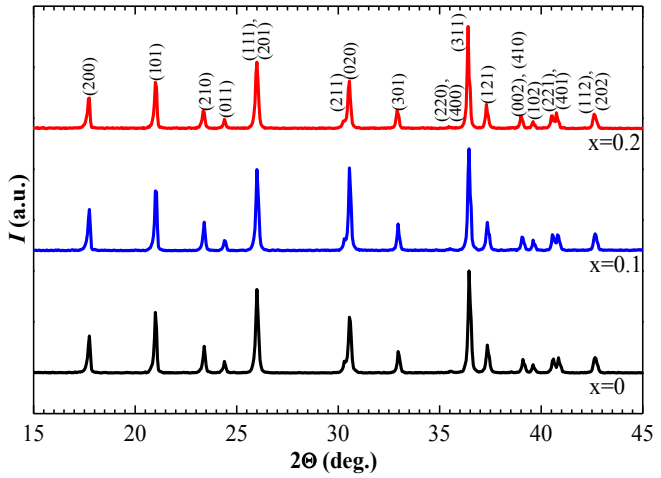

Figure 1. XRD patterns of $LiNi_{1-x}Co_xPO_4$ for x = (0, 0.1, and 0.2) at room temperature.

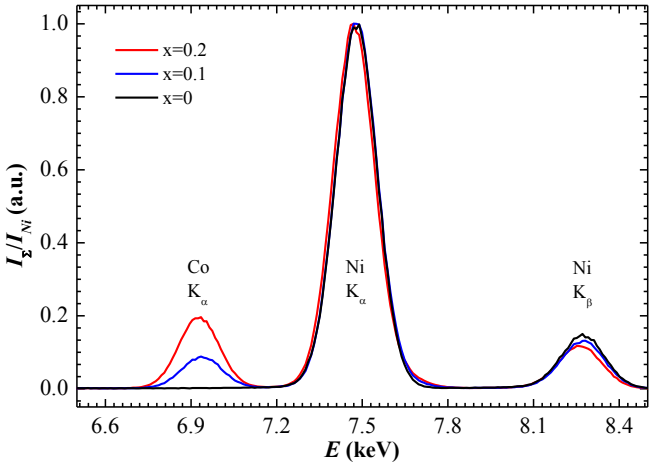

Figure 2. The normalized X-ray fluorescence spectra of the $LiNi_{1-x}Co_xPO_4$.

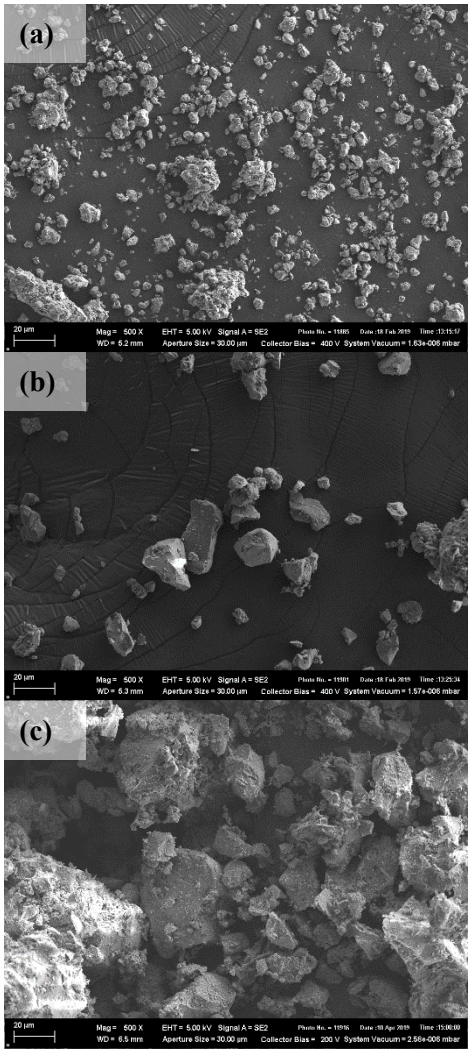

Figure 3. SEM-images of the $LiNi_{1-x}Co_xPO_4$ with x = 0 (a), 0.1 (b), and 0.2 (c). The scale factors are 20 μm.

Figure 4 presents temperature dependences of the magnetisation of $LiNi_{1-x}Co_xPO_4$ for x = (0, 0.1, and 0.2). The phase transition temperatures were determined from the temperature dependence of the first derivative of the magnetisation. For all samples the temperatures of C–IC antiferromagnetic phase transitions ($T_{C\text{-}IC}$) and Néel points (T_N) are distinctly observed.

The $T_{C\text{-}IC}$ and T_N temperatures for $LiNi_{1-x}Co_xPO_4$ magnetoelectrics are presented in Table 2. Here T_{max} is the temperature, at which the magnetization reaches maximum. All the $T_{C\text{-}IC}$, T_N, and T_{max} temperatures decrease with increasing the cobalt concentration and vice versa the value of the magnetization maximum increases. Such the behavior of the magnetic phase transitions is explained by a magnetic ordering competition. In the compounds with x = 0 and 1.0 the spins are oriented along

the *c*- and *b*-axis, respectively. The partial doping of $LiNi_{1-x}Co_xPO_4$ by cobalt ions leads to a narrowing of the temperature interval where the IC phase is established. The difference between temperatures T_N and T_{max} originates probably due to a disappearance of both long-range magnetic order above T_N and the short-range magnetic order above T_{max}.

Table 2. Temperatures of magnetic phase transitions in $LiNi_{1-x}Co_xPO_4$ magnetoelectrics and their maximum value of magnetization.

x	$T_{C\text{-}IC}$ (K)	T_N (K)	T_{max} (K)	M_{max} (emu/g)
0	20.86(2)	21.81(2)	24.29(3)	0.0419(1)
0.1	19.81(2)	20.47(2)	21.94(3)	0.0492(1)
0.2	18.63(2)	19.10(3)	19.89(4)	0.0638(1)

Figure 5 represents the NPD patterns of $LiNi_{0.9}Co_{0.1}PO_4$ at 10 K. In the *Pnma* space group the multiplicity of the general position is equal to 8. The 3d-transition metal ions at the 4*c* position with oxygen ions ($O1^{2-}$, $O2^{2-}$ are ions at the 4*c* position and four $O3^{2-}$ ions are at the 8*d* sites) together form the NiO_6 and CoO_6 octahedrons. The Li^+ ions form LiO_6 octahedrons with each pair of the $O1^{2-}$, $O2^{2-}$, and $O3^{2-}$ ions. Phosphorus ions are surrounded by PO_4 tetrahedrons ($O1^{2-}$, and $O2^{2-}$ ions, and two $O3^{2-}$ ions). The Li^+, M^{2+}, and P^{5+} ions are displaced from the geometric centres of the corresponding polyhedrons. At low temperatures the refined parameters of crystal structure of $LiNi_{0.9}Co_{0.1}PO_4$ are presented in Table 3. Within the uncertainty of measurements, the values of the structural parameters remain constant.

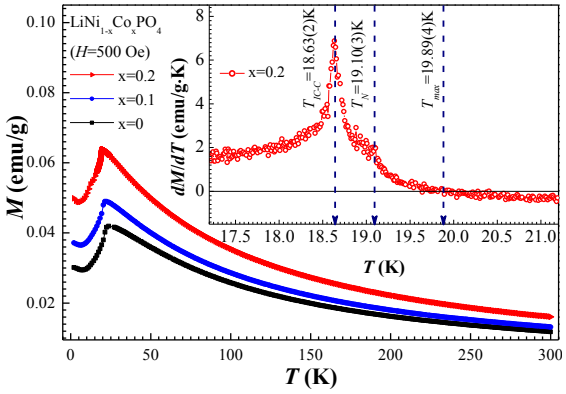

Figure 4. The temperature dependences of the magnetisation of $LiNi_{1-x}Co_xPO_4$ for x = (0, 0.1, and 0.2) under the applied magnetic field of 500 Oe. The inset presents the temperature dependence of the first derivative of the magnetisation for x = 0.2.

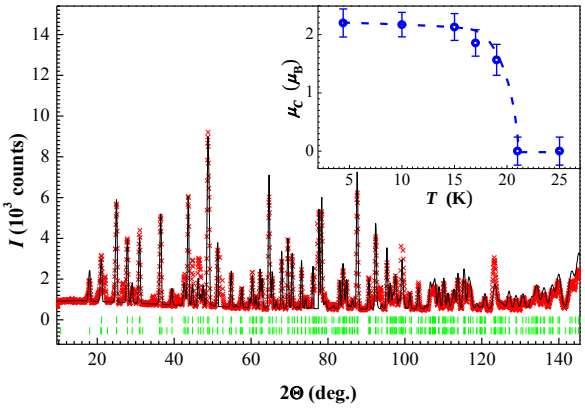

Figure 5. Observed (points) and calculated (line) NPD patterns of $LiNi_{0.9}Co_{0.1}PO_4$ at 10 K. The tick marks indicate the angle positions of nuclear and magnetic reflections. The inset shows the temperature dependence of the Ni/Co magnetic moments at 4*c* position for $LiNi_{0.9}Co_{0.1}PO_4$.

The C AFM structure of the $LiNi_{0.9}Co_{0.1}PO_4$ magnetoelectric is described by the propagation vector $\boldsymbol{k_C} = 0$. The insert at Figure 5 shows temperature dependence of the magnetic moment of Ni/Co ions at 4*c* position (μ_c) for x = 0.1. At low temperatures the μ_c moment magnitude is equal to about 2.2 μ_B, and then it decreases with temperature and vanishes at T_N. This corresponds to second-order magnetic phase transition.

Figure 6 presents the schematic visualization of magnetic structures calculated for C and IC models in $LiNi_{1-x}Co_xPO_4$ with propagation vectors $\boldsymbol{k_C} = 0$ ($\mu_c = 2.2\ \mu_B$) and $\boldsymbol{k_{IC}} = (0, \tau, 0)$ with $\tau = 0.12$ r.l.u. ($\mu_c = 1.2\ \mu_B$) [4], respectively.

Table 3. Crystallographic data for $LiNi_{0.9}Co_{0.1}PO_4$ at low temperatures. Parameters *a*, *b*, *c*, and *V* are the constants of the unit cell and its volume; *x*, *y*, and *z* are the ion coordinates;4*a*, 4*c*, and 8*d* are Wyckoff symbols. R_f and χ^2 are Bragg and global agreement factors.

Parameter	*T* = 10 K	*T* = 17 K	*T* = 21 K
a (Å)	10.035(1)	10.035(1)	10.035(1)
b (Å)	5.8550(7)	5.8551(7)	5.8549(8)
c (Å)	4.6728(5)	4.6727(5)	4.6725(7)
V (Å^3)	274.55(5)	274.56(5)	274.51(7)
Ni/Co, 4*c*: *x*	0.275(1)	0.275(1)	0.275(2)
z	0.987(4)	0.987(4)	0.987(2)
P, 4*c*: *x*	0.092(3)	0.092(3)	0.093(5)
z	0.412(6)	0.411(6)	0.411(7)
O1, 4*c*: *x*	0.099(3)	0.099(3)	0.100(3)
z	0.749(6)	0.749(6)	0.749(7)
O2, 4*c*: *x*	0.449(2)	0.449(2)	0.447(2)
z	0.212(6)	0.212(6)	0.209(7)
O3, 8*d*: *x*	0.166(2)	0.166(2)	0.167(2)
y	0.045(3)	0.045(3)	0.044(3)
z	0.289(4)	0.287(4)	0.289(4)
R_f (%)	4.7	4.6	4.9
χ^2 (%)	5.1	5.2	5.6

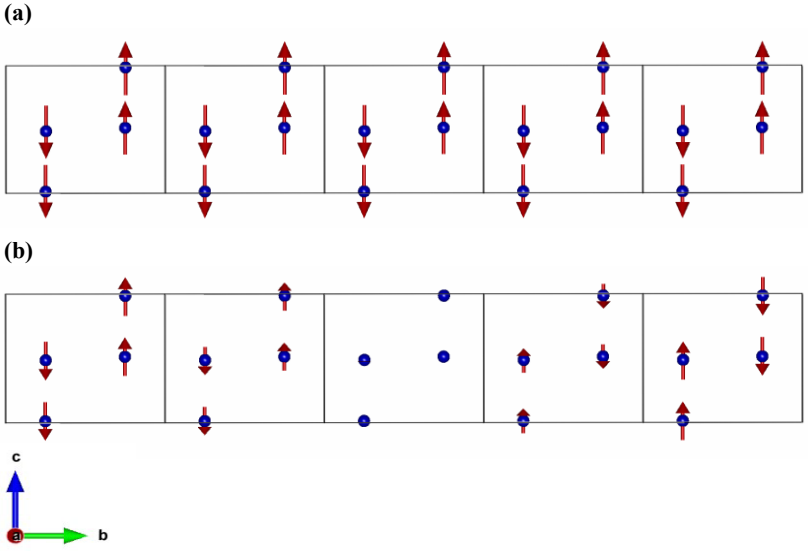

Figure 6. The C (a) and IC (b) models of AFM magnetic structures in $LiNi_{1-x}Co_xPO_4$ with propagation vectors $\boldsymbol{k_C} = 0$ and $\boldsymbol{k_{IC}} = (0, 0.12, 0)$, respectively (view on the *b*-*c* plate).

4. Conclusions

The partial doping in the $LiNi_{1-x}Co_xPO_4$ magnetoelectrics the Ni ions for Co ions leads to a narrowing of the temperature interval where the incommensurate phase is established.

The $T_{C\text{-}IC}$, T_N, and T_{max} temperatures of magnetic phase transitions decrease with rising cobalt concentration in $LiNi_{1-x}Co_xPO_4$, from 20.9 K, 21.8 K, and 24.3 K for x = 0, down to 19.8 K and 18.6 K ($T_{C\text{-}IC}$), 20.5 K and 19.1 K (T_N), 21.9 K and 19.9 K (T_{max}) for x = 0.1 and 0.2, respectively.

The difference between temperatures T_N and T_{max} originates probably due to a disappearance of both the long-range magnetic order above T_N and the short-range magnetic order above T_{max}.

Acknowledgments

The research was carried out within the state assignment of Minobrnauki of Russia (theme “Flux” No. AAAA-A18-118020190112-8 and theme “Magnet” No. AAAA-A18-118020290129-5).

The work was supported by MES of RF (contract No. 3.6121.2017/8.9), and by Act 211 Government of RF (contract No. 02.A03.21.0006).

The equipment of the Ural Center for Shared Use “Modern nanotechnology” SNSM UrFU was used.

References

[1] Pyatakov A P, Zvezdin A K 2012 *UFN* **182** 593 (In Russian)
[2] Cheong S W, Mostovoy M 2007 *Nat. Mat.* **6** 13
[3] Bibes M, Barthelemy A 2008 *Nat. Mat.* **7** 425
[4] Toft-Petersen R, Jensen J, Jensen T B S, Andersen N H, Christensen N B, Niedermayer C, Kenzelmann M, Skoulatos M, Le M D, Lefmann K, Hansen S R, Li J, Zarestky J L and Vaknin D 2011 *Phys. Rev.* B **84** 054408
[5] Rivera J-P 1994 *Ferroelec.* **161** 147
[6] Vaknin D, Zarestky J L, Rivera J-P and Schmid H 2004 *Phys. Rev. Lett.* **92**(20) 207201
[7] Kornev I, Bichurin M, Rivera J-P, Gentil S, Schmid H, Jansen A G M and Wyder P 2000 *Phys. Rev.* B **62**(18) 12247
[8] Urusova N, Semkin M, Kratochvilova M, Barykina J, Volegov A, Park J-G, Lee S, Pirogov A 2019 *J. All. and Comp.* **781** 571
[9] Semkin M, Choi K-Y, Sim H, Urusova N, Volegov A, Barykina J, Kellerman D, Park J-G and Pirogov A 2016 *AIP Conf. Proc.* **1767** 020035
[10] Vaknin D, Zarestky J L, Ostenson J E, Chakoumakos B C, Goñi A, Pagliuso P J, Rojo T and Barberis G E 1999 *Phys. Rev.* B **60**(2) 1100
[11] Toft-Petersen R, Andersen N H, Li H, Li J, Tian W, Bud'ko S L, Jensen T B S, Niedermayer C, Laver M, Zaharko O, Lynn J W and Vaknin D 2012 *Phys. Rev.* B **85** 224415
[12] Rodrigues-Carvajal J 1993 *Phys.* B **192** 55